Behavior of self-tapping screws used in hybrid light wood frame structures connected to a CLT core

Eini, A., Zhou, L., & Ni, C.

2022

buildings

MDPI

Article

Behavior of Self-Tapping Screws Used in Hybrid Light Wood Frame Structures Connected to a CLT Core

Ariya Eini [1,*], Lina Zhou [1] and Chun Ni [2]

[1] Department of Civil Engineering, University of Victoria, Victoria, BC V8P 5C2, Canada; linazhou@uvic.ca
[2] Building Systems, FPInnovations, Vancouver, BC V6T 1Z4, Canada; chun.ni@fpinnovations.ca
* Correspondence: ariyaeini@uvic.ca

Abstract: Light-frame wood structures are the most common type of construction for residential and low-rise buildings in North America. The 2015 edition of the National Building Code of Canada has increased the height limit for light-frame wood construction from 4 to 6 stories. With the increase in building height, it was noticed that light-frame wood structures may be governed by inter-story drift under wind and seismic loads. To reduce the inter-story drift, a hybrid system, consisting of CLT cores and light-frame structures, is proposed. The efficiency of this hybrid system is dependent on the performance of the connections between the two sub-systems. In this project, self-tapping screws (STSs) were used to connect the CLT core and light-frame wood structures on the floor level. Monotonic and reversed-cyclic tests were carried out on CLT-wood frame connections connected with STSs inserted at 45°, 90°, and mixed angles (45° and 90°). The connection performance was evaluated in terms of strength, stiffness, ultimate displacement, ductility, and energy dissipation capacity. Results show that a joint with STSs inserted at 45° had high stiffness and ductility but low energy dissipation, while connections with STSs installed at 90° had high ductility and energy dissipation but low stiffness. Connections with STSs inserted at mixed angles (45° and 90°) achieved the advantages of both configurations when the STSs were inserted at 45° or 90° individually, i.e., high stiffness, ductility, and energy dissipation. The ductility and energy dissipation were significantly improved compared with connections with STSs only inserted at 45° or 90°. This mixed angle connection can be an ideal design for connecting light-frame wood structures to a CLT core to resist wind and seismic load.

Keywords: light-frame wood structure; cross-laminated timber; self-tapping screw; monotonic test; reversed-cyclic test; connection capacity; ductility

Citation: Eini, A.; Zhou, L.; Ni, C. Behavior of Self-Tapping Screws Used in Hybrid Light Wood Frame Structures Connected to a CLT Core. *Buildings* **2022**, *12*, 1018. https://doi.org/10.3390/buildings12071018

Academic Editor: Jorge Manuel Branco

Received: 11 June 2022
Accepted: 11 July 2022
Published: 14 July 2022

1. Introduction

Traditional light-frame wood buildings have proven to be a practical and sustainable solution for residential construction. The height limit of light-frame wood construction has been increased from four to six stories in the National Building Code of Canada (NBCC) [1]. With the increase in building height, these structures become more flexible and may have large lateral deformation under wind and seismic loads. As a result, the drift requirements may be hard to meet for the design of mid-rise wood frame buildings. Elevator shafts and stairwells commonly exist in multi-story buildings and can be used as part of the lateral load resisting system to reduce the lateral drift of the wood frame system. Cross-Laminated Timber (CLT) core has become more popular in multi-story light-frame wood buildings due to its fast construction compared with a reinforced concrete or masonry core. This core can provide the building with additional lateral load resistance, if sufficiently connected to the wood frame, and reduce the lateral deformation [2]. In this project, a hybrid system consisting of a light-frame wood structure connected to a CLT core was proposed. CLT cores are connected to light-frame structures on the floor level as shown in Figure 1a, where light-frame wood shear walls dissipate energy through deformation of the sheathing-to-framing nail joints [3], while CLT panels are rigid and rely on the panel-to-panel and

panel-to-foundation connections to provide ductility [4]. Therefore, connections between the two sub-systems play an important role in the performance of the hybrid structure and can be used as one source of energy dissipation for seismic design if ductile performance is achieved through detailed design. In this project, self-tapping screws were used to transmit lateral loads between the two sub-systems.

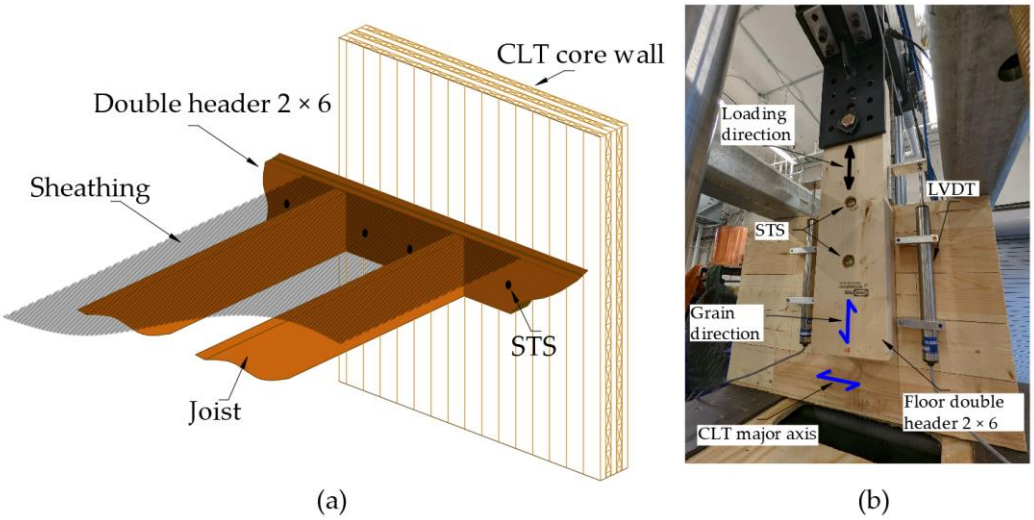

Figure 1. Self-tapping screw connections: (**a**) schematic of STS connections used in CLT and light-frame wood hybrid systems; (**b**) test specimen setup.

Previous studies on CLT light-frame wood hybrid structures have been very limited. Nguyen et al. [5] tested a hybrid shear wall system consisting of wood frame shear wall segments and post-tensioned CLT panels. The CLT wall was connected to the studs of the wood frame shear wall using common nails. Test results showed that this hybrid wall system had high stiffness, energy dissipation, and a self-centering capability. Anandan et al. [6] conducted a full-scale shake table test on a one-story post-tensioned CLT building. Additional wood frame shear walls were connected to the CLT floor diaphragm through threaded steel rods. The hybrid system was tested under the 1994 Northridge earthquake, with a hazard level of 10% and a 2% probability of exceedance in 50 years, which corresponds to design-basis earthquake (DBE) and maximum considered earthquake (MCE), respectively. Results showed that the system was able to recenter itself after shaking. The sheathing of the wood frame was marginally shifted after DBE excitation. The wood frame sustained moderate damage under MCE excitation.

Self-tapping screws (STSs) are commonly used in CLT construction [7]. With relatively higher capacity compared with dowel-type connections, STSs are very efficient in resisting lateral and axial loads for timber-to-timber connections [8]. There has been much research conducted on the STSs used in CLT structures. Munoz et al. [9] studied typical CLT floor-to-floor and wall-to-floor connections connected with STSs. Results showed that lap connections using STSs had better lateral capacity, stiffness, and ductility than spline configurations with normal wood screws. Hossain et al. [10] studied the performance of STS connections connecting 3-ply CLT panels under cyclic and monotonic loading. They found that STS connections with mixed angles had high stiffness and ductility. Tomasi et al. [11] also confirmed the superior performance of STSs installed with mixed angles in glued laminated timber joints. Gavric et al. [12] performed reversed-cyclic tests on different configurations of STS connections used in coupled CLT wall panels. They concluded that 90° STSs can achieve high ductility if sufficient spacing is provided. Brown et al. [13] investigated the behavior of STS joints between CLT panels with varying ratios of STSs installed inclined and at 90° to the timber grain. They found that a ratio of 2:1 yielded more efficient design. These studies were all focused on CLT-to-CLT or CLT-to glulam connections. There has been no investigation on CLT shear wall-to-light-frame wood floor,

i.e., CLT-lumber connections connected with STSs. In this project, cyclic and monotonic tests were conducted on CLT-lumber STS connections to assess the stiffness, load-carrying capacity, ductility, and energy dissipation capacity of this connection. In order to obtain a ductile connection system, CLT-lumber connections with different STS insertion angles were investigated.

2. Test Program

Figure 1a shows a schematic of the CLT-lumber connection. The CLT wall panel was directly connected to the floor headers of light-frame wood structures with STSs. Figure 1b shows the test setup of the connection specimen. Five-layer CLT panels with a thickness of 175 mm were used in this project. The panel had an E1 stress grade according to ANSI/APA PRG 320 [14] and was made of Spruce-Pine-Fir (SPF) machine stress rated lumber in longitudinal layers and No. 3/Stud SPF lumber in transverse layers [15]. Table 1 shows the mechanical properties of E1 stress grade CLT panels cited from ANSI/APA PRG 320 [14] as no material tests were performed in this project. Three types of connection configurations with different STS insertion angles were studied, i.e., STS inserted at 90° (Figure 2a), 45° (Figure 2b), and mixed angles (90° and 45°) (Figure 2c) to the grain of the lumber (hereafter named 90° STS, 45° STS, and mixed angle STS). Two diameters of ASSY® SK and VG CSK STSs made from carbon steel (8 and 10 mm) were tested (Figure 2d). The mechanical properties of STSs cited from the CCMC report [16] are listed in Table 1. The 90° STS loaded in shear was partially threaded (PT) and 160 mm long, and the 45° STS loaded in both shear and withdrawal was fully threaded (FT) and 240 mm long. The floor header was composed of double 2 × 6 SPF lumber. For the 90° STS or 45° STS connections, each specimen had 2 screws. The mixed angle (90° and 45°) connection had two screws installed at 45° and the other two installed at 90°. Screws penetrated around two and a half layers into the CLT panel for all cases. Initially, 10d (d = 10 mm) was used as the screw spacing and end distance for both diameter screws. However, with the splitting of lumber in two replicates of STS connections with 10 mm diameter screws inserted at 90° under monotonic load, it was decided that 12d and 15d (d = 10 mm) be used for screw spacing and end distance, respectively, according to the MTC Solution Handbook [17].

Table 1. Material properties.

CLT [14]	**Layers**	
	Longitudinal	**Transversal**
Bending at extreme fibre, f_b (MPa)	28.2	7.0
Longitudinal shear, f_v (MPa)	1.5	1.5
Rolling shear, f_s (MPa)	0.5	0.5
Compression parallel to grain, f_c (MPa)	19.3	9.0
Compression perpendicular to grain, f_{cp} (MPa)	5.3	5.3
Tension parallel to grain, f_t (MPa)	15.4	3.2
Modulus of elasticity, E (MPa)	11700	9000
Shear modulus, G (MPa)	731	563
Longitudinal shear, f_v (MPa)	73.1	56.3
STS [16]	**Diameter**	
	8 mm	**10 mm**
Bending yield strength (MPa)	1015	942
Unfactored tension strength (kN)	18.9	24
Unfactored shear strength (kN)	641	691

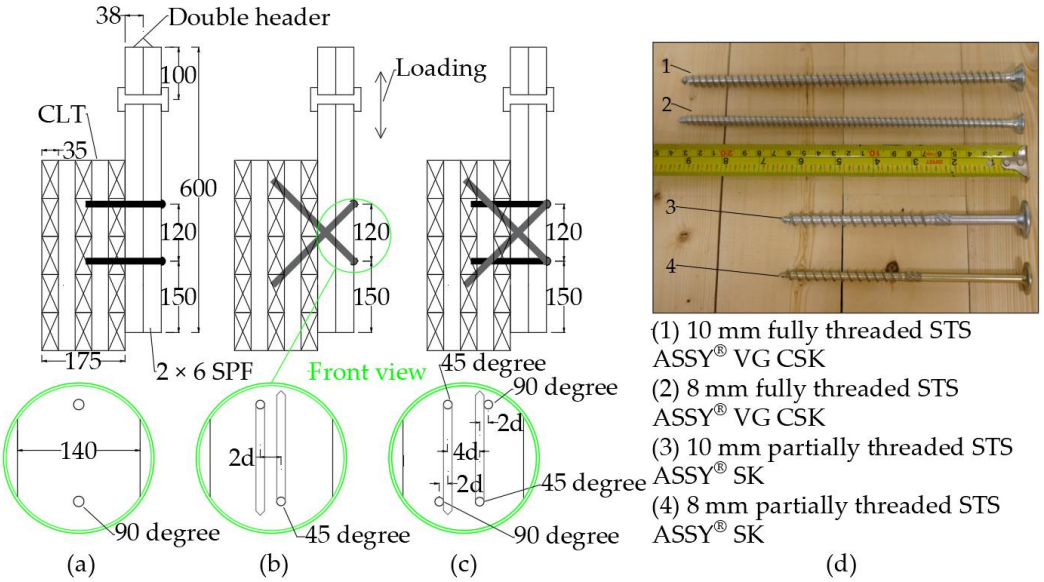

Figure 2. STS connection configurations (mm): (**a**) 90° STS; (**b**) 45° STS; (**c**) mixed angle (45° and 90°) STS; (**d**) self-tapping screws.

In the proposed hybrid system, lateral forces were assumed to be transferred between the CLT core and floor header through the STSs. Cyclic and monotonic loadings were applied parallel to the grain of the lumber (Figure 1b). A summary of tested series is provided in Table 2. Four replicates were tested for each configuration, and there were 48 specimens tested in total. According to ASTM 1761-20 [18], the speed of the monotonic and cyclic test was set to 0.05 and 2 mm/s, respectively. Test method C (CUREE) [19] was used to define the loading protocol of the reversed-cyclic tests. The reference deformation of the CUREE protocol was derived based on monotonic test results, which were 3.6 and 30 mm for the 45° and 90° STS connection test, respectively. To measure the relative displacement between lumber and the CLT panel, two Linear Variable Differential Transformers (LVDTs) were attached to both sides of the lumber, as shown in Figure 1b. Prior to testing, lumbers were conditioned in an environmental room with 20° C and 65% relative humidity until they reached equilibrium moisture content (EMC). Lumber with relative density within 0.4 ± 0.04 were used in this project.

Table 2. Test matrix.

Loading Type	STS Insertion Angle	STS Type	Diameter of Fasteners (mm)	Length of Fasteners (mm)
Monotonic	90°	PT [1]	8	160
			10	160
	45°	FT [2]	8	240
			10	240
	45° + 90°	FT + PT	8	160 + 240
			10	160 + 240
Cyclic	90°	PT	8	160
			10	160
	45°	FT	8	240
			10	240
	45° + 90°	FT + PT	8	160 + 240
			10	160 + 240

Notes: [1]: partially threaded. [2]: fully threaded.

3. Experimental Results

Displacement from both LVDTs was averaged. Data was recorded at a frequency of 10 and 100 Hz for the monotonic and cyclic tests, respectively. An example of cyclic load-deformation curves is shown in Figure 3a–c. It can be seen that both 90° STS and mixed angle STS connections achieved large displacement at around 30 mm without significant reduction in resistance, while the 45° STS connection had higher resistance compared with the 90° STS but failed at much smaller displacement. Figure 3d,e shows comparisons of individual backbone curves for each connection configuration and the superposition of 45° STS and 90° STS curves under cyclic and monotonic load, respectively. It can be seen that the shape of the superposition curve and mixed angle connection curve were similar, which indicates that in the mixed angle connection, 45° STSs mostly contribute to the initial stiffness and 90° STSs mainly contribute to the ultimate displacement. There was a clear drop-down phase of the curve in the mixed angle connection when the 45° STSs withdrew from the CLT panel. After that, the resistance recovered and further increased when the 90° STSs contributed more resistance due to redistribution of the load between the two groups of fasteners.

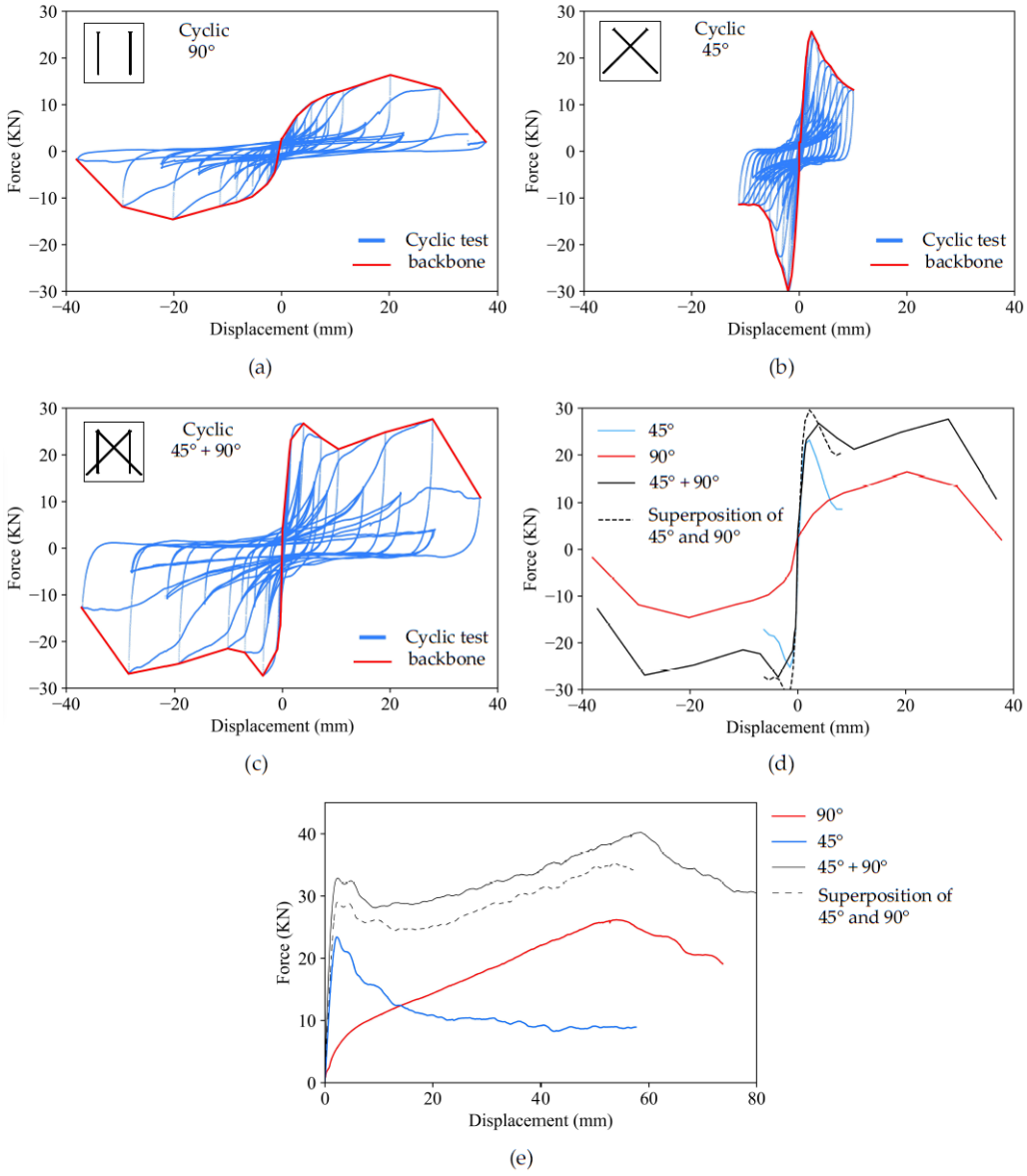

Figure 3. Load-displacement curves for 8 mm STSs (single replicate data): (**a**) 90° STS; (**b**) 45° STS; (**c**) mixed angle STS; (**d**) cyclic backbone curves; (**e**) monotonic curves.

The positive and negative backbones of the cyclic tests were averaged. All the averaged backbone and monotonic curves of tests with their associated failure points are shown in Figure 4. Failure was defined when the load dropped to 80% of the maximum resistance. In the case of the mixed angle connections, failure was defined after the second peak load when the 90° STSs also lost their resistance. Although in some cases there was a 20% drop-down after the first peak when the 45° STSs lost their resistance, the overall resistance of the mixed angle connections was recovered due to redistribution of forces between the two groups of fasteners. The drop-down amount after the first peak can be optimized by adjusting the ratio of 45° STSs over 90° STSs [13]. As shown in Figure 4, two specimens of 10 mm STSs inserted at 90° under monotonic load (10d screw spacing, 10d end distance, and 7d edge distance) and one specimen of 10 mm STS inserted at 90° under cyclic load (12d screw spacing, 15d end distance, and 7d edge distance) failed at much smaller ultimate displacement than the other replicates. One specimen of 8 mm STS inserted at mixed angles (12d screw spacing, 15d end distance, and 3d edge distance) failed at a slightly smaller displacement than the other replicates. These failures happened because of splitting in the lumber (Figure 5d,e). In the other cases, wood only showed localized crushing around the STSs (Figure 5a–c). Therefore, connections with lumber splitting showed a less ductile behavior compared with the other replicates. With larger end distances or predrilling, this failure may be prevented. In general, 10 mm STS connections have higher resistance and are more prone to splitting wood than 8 mm STS connections. Mixed angle and 90° STS connections failed at much smaller displacement under cyclic load compared to those under monotonic load; however, there was not much difference for 45° STS connections.

Using the Equivalent Energy Elastic-Plastic [19] method, the mechanical properties of CLT-lumber STS connections were obtained. The ultimate displacement was defined as the displacement at 80% of the maximum load on the descending phase (after the second peak in the case of mixed angle connections) (Figure 4) [19]. The mean and coefficient of variation (COV) of these properties were: yield force (F_y) and its corresponding yield displacement (Δ_y), peak force (F_{peak}) and its corresponding displacement (Δ_{peak}), ultimate displacement (Δ_u), stiffness (K), ductility (μ), and energy dissipation (E). These are presented in Tables 3 and 4 for monotonic and cyclic loading. Comparison of the mean values of these mechanical properties is shown in Figure 6. Specimens with STSs installed at 90° had larger ultimate displacement (around 70 mm under monotonic load and 30 mm under cyclic load) than that of STSs inserted at 45° (around 5 mm under both monotonic and cyclic loads). Interestingly, although the 90° STS connections had much larger ultimate displacement, the ductility was similar to that of the 45° STS connections. This is because the 45° STS is much stiffer than the 90° STS, so the yield displacement of STSs inserted at 45° (around 1.1 mm under both monotonic and cyclic loads) was much smaller than STSs inserted at 90° (around 17 mm under monotonic and 6 mm under cyclic load). Therefore, the ratio of ultimate displacement to yield displacement (i.e., ductility value) was similar for these two groups of connections. It is worth mentioning this conclusion is dependent on the definition of the ductility ratio. Despite having similar ductility, 90° STS connections have higher energy dissipation capacity than that of 45° STS connections (more than six times under monotonic load and 1.9 times under cyclic load). For the mixed angle STS (45° and 90°) connections, small yield displacement and large ultimate displacement are both presented. Accordingly, the ductility of the specimens with mixed angle connections greatly increased (around 56 under monotonic and 32 under cyclic load) compared with connections with 90° STSs or 45° STSs. Mixed angle STS connections had an energy dissipation of more than 11 times the value of 45° STS connections. This effect was more pronounced in 8 mm STSs compared with 10 mm STS specimens. The 45° STS connection had on average more than 50% load-carrying capacity (52% for 10 mm STSs and 64% for 8 mm STSs) compared with 90° STS under cyclic loading. However, it had relatively less capacity under monotonic loading. Connections with mixed 45° and 90° STSs had higher peak resistance compared with that with 90° STSs or 45° STSs only but less than the sum of the resistance of the two connections. This is because the 45° STSs and 90° STSs in the mixed angle connections did not reach their peak resistance at the same

displacement. A transition of load sharing between 45° STSs and 90° STSs was observed in mixed angle connections.

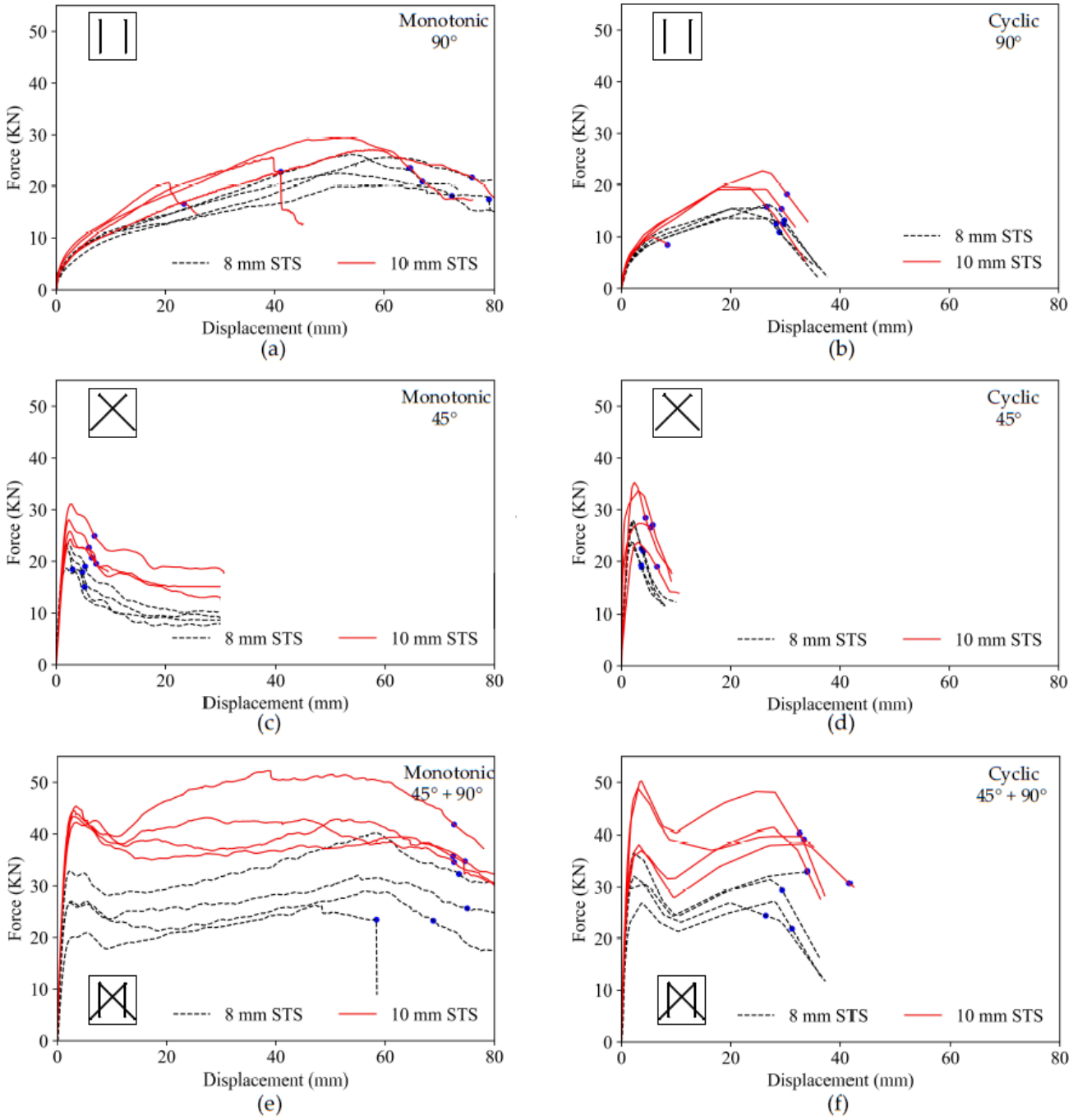

Figure 4. Cyclic backbones and monotonic curves of STS connections: (**a**) 90° STS under monotonic; (**b**) 90° STS under cyclic; (**c**) 45° STS under monotonic; (**d**) 45° STS under cyclic; (**e**) mixed angle (45° and 90°) STS under monotonic; (**f**) mixed angle (45° and 90°) STS under cyclic. **Notes:** Failure points are marked with dots at 80% of maximum load on the descending phase.

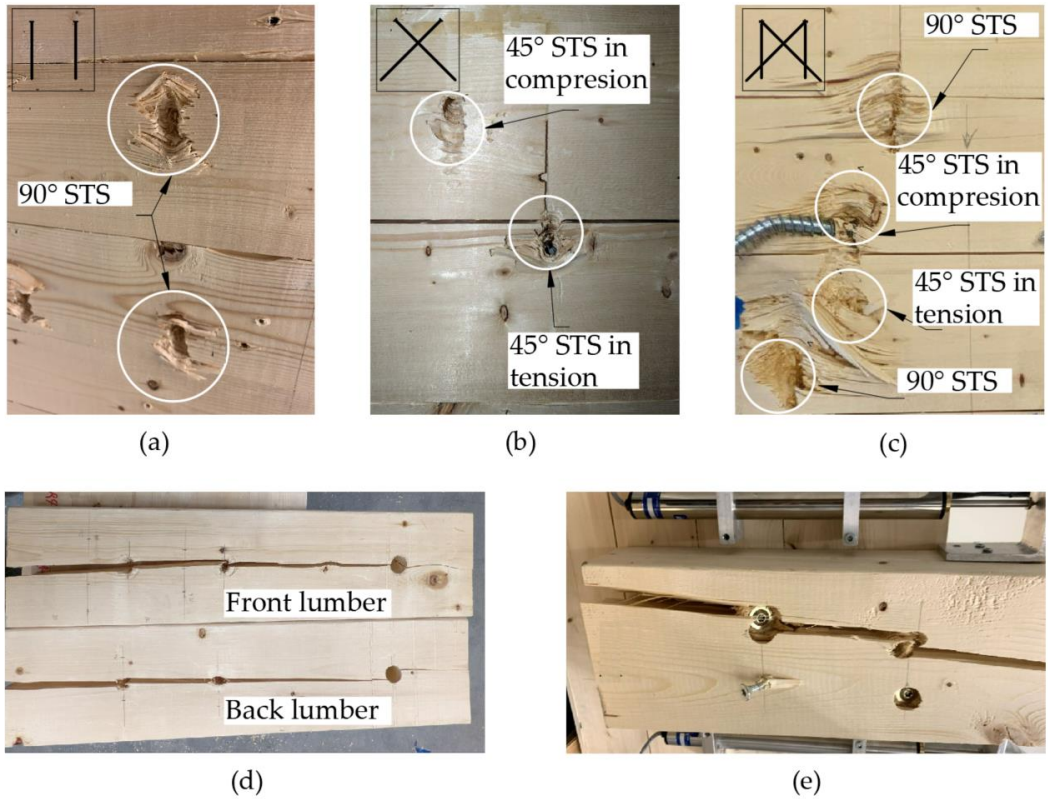

Figure 5. Failure on wood: (**a**) wood crush in 90° STSs; (**b**) wood crush in 45° STSs; (**c**) wood crush in mixed angle connection (90° and 45°); (**d**) wood splitting in 10 mm connection with STSs installed at 90°; and (**e**) wood splitting in 8 mm connection with STSs installed at mixed angles (90° and 45°).

Table 3. Mechanical properties of STS connections under monotonic loading.

Monotonic	Screw Diameter	Δ_y (mm)	F_y (kN)	F_{peak} (kN)	Δ_{peak} (mm)	Δ_u (mm)	K (kN/mm)	μ	E^2 (kN·mm)
90°	8 mm	18.4	21.1	26.2	53.9	66.9	1.1	3.6	1217.5
		22.4	20.6	25.7	61.1	86.1	0.9	3.9	1542.9
		12.3	18.8	22.6	52.0	72.3	1.5	5.9	1243.6
		8.7	16.6	20.3	61.7	79.1	1.9	9.1	1240.9
	Mean	15.4	19.2	23.7	57.2	76.1	1.4	5.6	1311.2
	COV	34%	9%	10%	8%	10%	27%	39%	10%
45°	8 mm	0.9	20.6	22.9	1.7	3.1	23.9	3.6	54.6
		1.0	20.0	22.2	2.0	4.8	21.0	5.1	86.0
		1.3	21.2	23.4	2.2	5.4	16.0	4.1	100.7
		0.9	17.5	18.6	1.9	5.2	19.4	5.8	83.1
	Mean	1.0	19.8	21.8	1.9	4.6	20.1	4.6	81.1
	COV	18%	7%	9%	9%	20%	14%	19%	21%
45° + 90°	8 mm	1.12	24.9	29.0	56.5	68.8	22.2	61.5	1699.2
		1.18	27.6	32.0	55.2	75.0	23.3	63.4	2053.7
		1.63	22.1	26.3	47.4	58.5	13.5	35.9	1274.8
		1.17	33.4	40.2	58.4	73.6	28.5	62.9	2438.7

Table 3. *Cont.*

Monotonic	Screw Diameter	Δ_y (mm)	F_y (kN)	F_{peak} (kN)	Δ_{peak} (mm)	Δ_u (mm)	K (kN/mm)	μ	E [2] (kN·mm)
	Mean	1.28	27.0	31.9	54.4	69.0	21.9	55.9	1866.6
	COV	16%	16%	16%	8%	9%	25%	21%	23%
90°	10 mm	20.8	22.7	27.2	57.3	75.9	1.1	3.7	1486.9
		14.1 [1]	21.1 [1]	25.7 [1]	39.3 [1]	41.1 [1]	1.5 [1]	2.9 [1]	718.5 [1]
		5.6 [1]	16.2 [1]	20.8 [1]	20.7 [1]	23.3 [1]	2.9 [1]	4.2 [1]	332.1 [1]
		16.0	24.6	29.4	52.6	64.7	1.5	4.0	1394.8
	Mean	18.4	23.6	28.3	42.5	70.3	1.3	3.8	1440.8
	COV	13%	4%	4%	33%	8%	17%	5%	3%
45°	10 mm	1.4	25.4	28.0	2.3	6.1	17.5	4.2	137.2
		1.5	28.3	31.1	2.7	7.0	18.7	4.6	176.9
		1.5	23.0	25.8	2.5	6.5	15.2	4.3	132.3
		1.5	22.3	24.3	2.6	7.3	14.7	4.8	146.1
	Mean	1.5	24.8	27.3	2.5	6.7	16.5	4.5	148.1
	COV	2%	9%	9%	6%	7%	10%	5%	12%
45° + 90°	10 mm	1.21	39.3	44.5	51.0	72.4	32.5	59.9	2821.5
		1.15	37.4	43.4	63.1	74.6	32.5	64.9	2768.5
		1.30	40.3	43.2	44.8	72.7	31.1	55.9	2903.6
		1.53	47.5	52.3	38.6	72.6	31.1	47.5	3412.2
	Mean	1.30	41.1	45.8	49.4	73.1	31.8	57.1	2976.5
	COV	11%	9%	8%	18%	1%	2%	11%	9%

Notes: [1] The specimen failed due to splitting of wood, and its mechanical properties are not used in calculation of mean and COV. [2] Energy dissipation under monotonic load is calculated to the failure point (Figure 4). The energy dissipation under cyclic load is calculated to the end of the first primary cycle that causes drop of the peak resistance below 80% of the maximum load. The two subsequent cycles with 75% amplitude are not included.

Table 4. Mechanical properties of STS connections under reversed-cyclic loading.

Cyclic	Screw Diameter	Δ_y (mm)	F_y (KN)	F_{peak} (KN)	Δ_{peak} (mm)	Δ_u (mm)	K (kN/mm)	μ	E [2] (kN·mm)
90°	8 mm	6.1	13.0	16.6	26.8	29.8	2.1	4.9	550.6
		4.2	11.8	14.4	26.2	28.3	2.8	6.7	495.8
		5.4	13.3	16.7	26.5	27.9	2.5	5.2	530.3
		4.4	13.0	15.5	20.2	29.7	3.0	6.8	520.6
	Mean	5.0	12.8	15.8	24.9	28.9	2.6	5.9	524.3
	COV	15%	4%	6%	11%	3%	13%	15%	4%
45°	8 mm	1.0	21.5	23.9	2.5	4.3	21.9	4.4	174.8
		1.1	25.5	28.1	2.0	3.8	23.6	3.5	150.2
		1.2	24.9	27.8	2.2	3.9	20.5	3.2	174.1
		0.8	22.1	24.2	1.8	3.5	27.0	4.3	151.4
	Mean	1.0	23.5	26.0	2.1	3.9	23.2	3.9	162.6
	COV	14%	7%	8%	12%	7%	10%	13%	7%

Table 4. *Cont.*

Cyclic	Screw Diameter	Δ_y (mm)	F_y (KN)	F_{peak} (KN)	Δ_{peak} (mm)	Δ_u (mm)	K (kN/mm)	μ	E [2] (kN·mm)
45° + 90°	8 mm	0.92	29.4	32.9	34.1	34.1	32.0	37.1	2214.5
		0.81	24.2	27.2	27.9	31.3	30.0	38.8	2184.1
		0.91	29.3	36.6	27.5	29.5	32.2	32.5	2411.4
		1.11	26.0	30.6	19.9	26.5	23.4	23.9	2409.2
	Mean	0.94	27.2	31.8	27.4	30.4	29.4	33.1	2304.8
	COV	12%	8%	11%	18%	9%	12%	17%	5%
90°	10 mm	7.0	17.3	20.9	26.4	30.0	2.5	4.3	621.5
		8.3	18.6	23.0	25.8	30.3	2.2	3.7	663.4
		5.4	16.8	20.9	23.5	25.8	3.1	4.7	608.3
		1.8 [1]	9.1 [1]	10.4 [1]	8.0 [1]	9.0 [1]	5.2 [1]	5.2 [1]	163.0 [1]
	Mean	6.9	17.6	21.6	25.2	28.7	2.6	4.2	631.1
	COV	17%	4%	5%	36%	7%	13%	10%	4%
45°	10 mm	1.5	31.8	35.7	2.3	4.8	21.9	3.3	250.0
		0.7	35.1	39.5	0.6	4.0	52.6	6.0	261.1
		0.9	28.8	32.2	1.0	5.8	32.9	6.6	300.0
		1.5	21.4	23.8	3.2	6.6	14.3	4.4	252.3
	Mean	1.1	29.3	32.8	1.8	5.3	30.4	5.1	265.8
	COV	32%	17%	18%	59%	18%	47%	26%	8%
45° + 90°	10 mm	1.10	34.5	38.3	33.6	41.7	31.2	37.7	3052.6
		1.15	39.9	48.9	24.8	33.5	34.8	29.2	3252.6
		1.17	44.9	50.2	27.1	32.7	38.4	27.9	3326.7
		1.06	36.6	41.3	27.5	34.1	34.4	32.0	2614.9
	Mean	1.12	39.0	44.7	28.2	35.5	34.7	31.7	3061.7
	COV	4%	10%	11%	11%	10%	7%	12%	9%

Notes: [1] The specimen failed due to splitting of wood and its mechanical properties are not used in calculation of mean and COV. [2] Energy dissipation under monotonic load is calculated to the failure point (Figure 4). The energy dissipation under cyclic load is calculated to the end of the first primary cycle that causes drop of the peak resistance below 80% of the maximum load. The two subsequent cycles with 75% amplitude are not included.

There was a high variance in the stiffness of 10 mm STSs inserted at 45° under cyclic load (Table 4). This was due to the eccentric installation of STSs. There was a 2d offset (Figure 2b) between the two 45° STSs, which led to twisting in the lumber. Figure 7 demonstrates the failure modes of self-tapping screws under monotonic and cyclic loads. All specimens with STSs inserted at 90° showed two yielding points under monotonic loading, but all of them broke at these two points under cyclic loading. The breaking of 90° STSs under cyclic load was due to the cumulated damage in plastic deformation, which causes reduction of the ultimate displacement under cyclic load compared with that under monotonic load (Tables 3 and 4). In 45° STS connections, one of the screws inserted at 45° broke due to a combination of compression and shear, and the other yielded in shear and was withdrawn under monotonic loading. When loaded under reversed-cyclic load, all STSs inserted at 45° were slightly bent at two points. Therefore, the ultimate displacement of STSs inserted at 45° under cyclic load was similar to that under monotonic load (Tables 3 and 4). The 45° STS broken because of the combination of compression and shear under monotonic load may have been due to buckling. Similarly, the 45° STSs in mixed angle connections remained unbroken and slightly bent, while the 90° STSs were broken under cyclic tests. Specimens with mixed angle STSs had the same failure modes as individual 45° STS and 90° STS connections under monotonic loading.

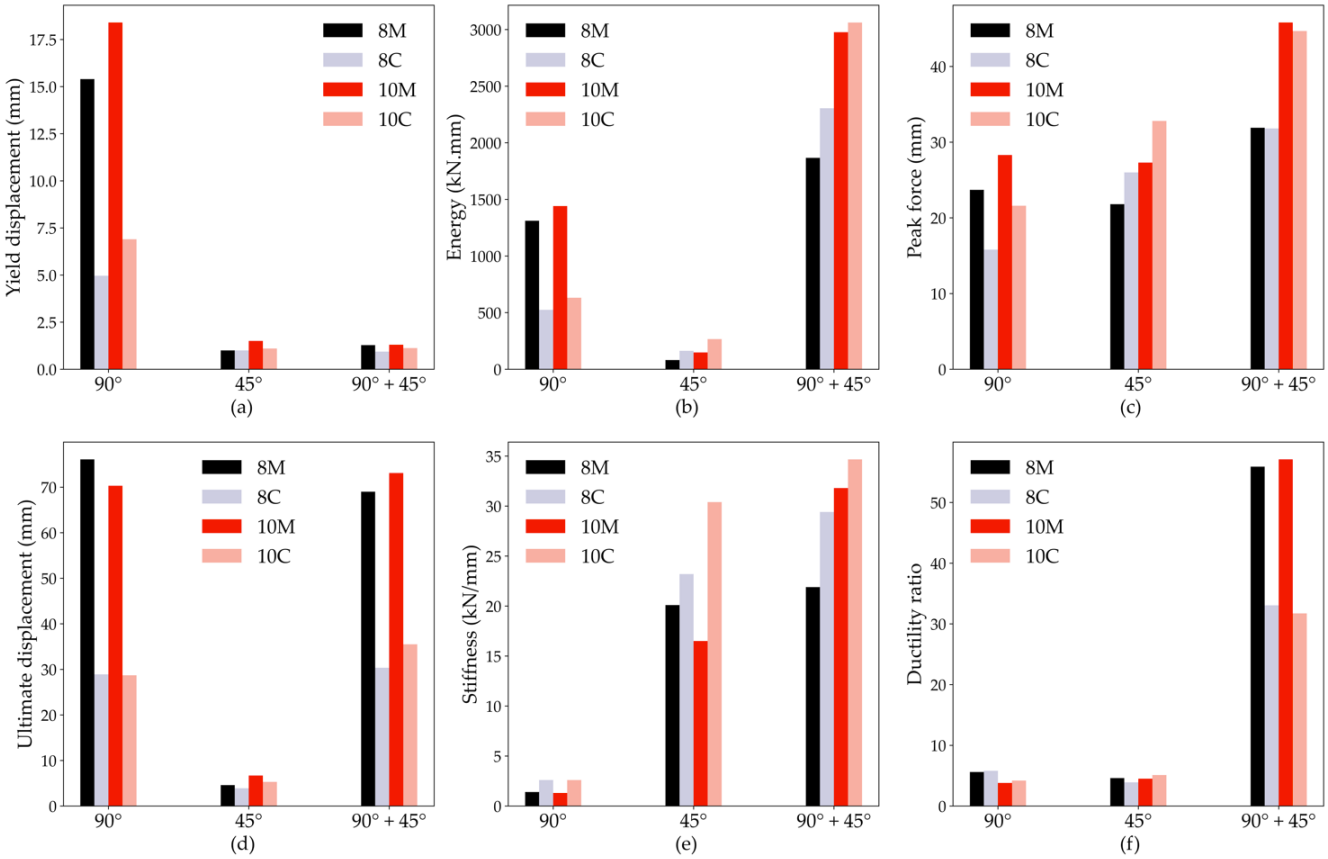

Figure 6. Comparison of average mechanical properties of STS connections: (**a**) yield displacement; (**b**) energy dissipation; (**c**) peak force; (**d**) ultimate displacement; (**e**) stiffness; (**f**) ductility ratio.

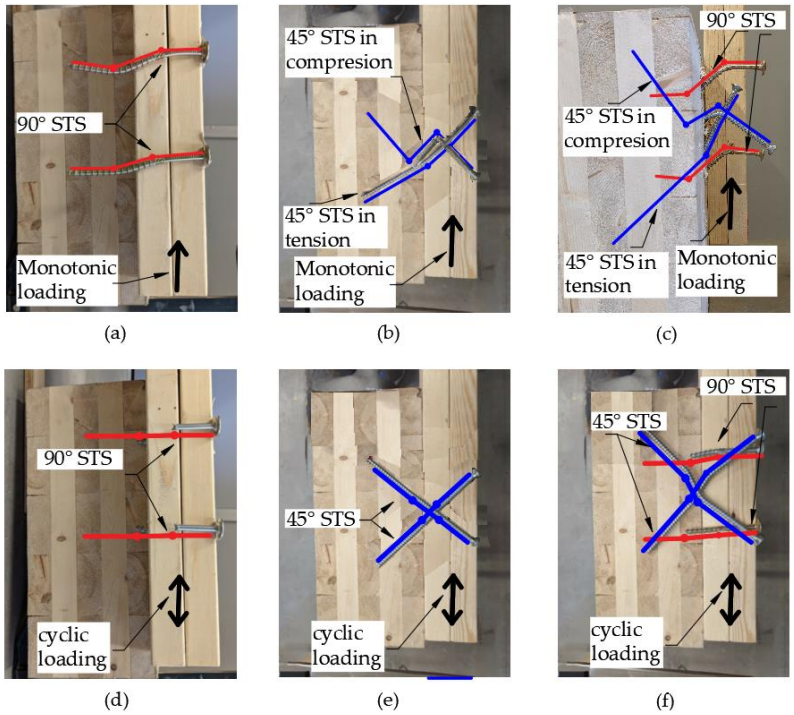

Figure 7. Failure modes of STSs in CLT-lumber connections: (**a**) 90° STS; (**b**) 45° STS; (**c**) mixed angle STS (45° and 90°); (**d**) STS at 90°; (**e**) STS at 45°; and (**f**) STS at mixed angles (90° and 45°).

The relationship between energy dissipation and ductility is not usually straightforward. The total energy dissipation depends largely on the displacement history, i.e., the loading protocol. However, the ductility is sensitive to the yielding displacement or initial stiffness. Therefore, another parameter commonly used for evaluation of the energy dissipation capacity of a system, the equivalent viscous damping, is calculated for each cycle of the hysteresis loops using Equation (1) [20].

$$\zeta_{hyst} = \zeta_{eq.viscous} = \frac{A_{half-loop}}{\pi.F_{max}.D_{max}} \quad (1)$$

where $A_{half\text{-}loop}$ is half of the energy dissipated in each hysteresis loop. F_{max} and D_{max} are the maximum force and displacement of the same loop, respectively.

Equivalent viscous damping characterizes the energy dissipation due to plastic behavior. As shown in Figure 8, before yielding, the equivalent viscous damping was more than 10% for connections with 90° STSs, but for connections with 45° STSs and mixed angle connections, damping was smaller. At higher displacement, the equivalent viscous damping reached up to at least 20% for all configurations, which indicates good energy dissipation capacities of these connections. This conclusion seems neither consistent with what is derived based on ductility ratio nor energy dissipation. This is because the equivalent hysteretic damping is proportional to the energy dissipation normalized with the peak load and its corresponding displacement on each cycle (see Equation (1)), which is different from the value of total energy dissipation and ductility ratio. Further research should be carried out on the energy dissipation capacity of the three types of STS connections used in a hybrid CLT-wood frame structure through time history analysis.

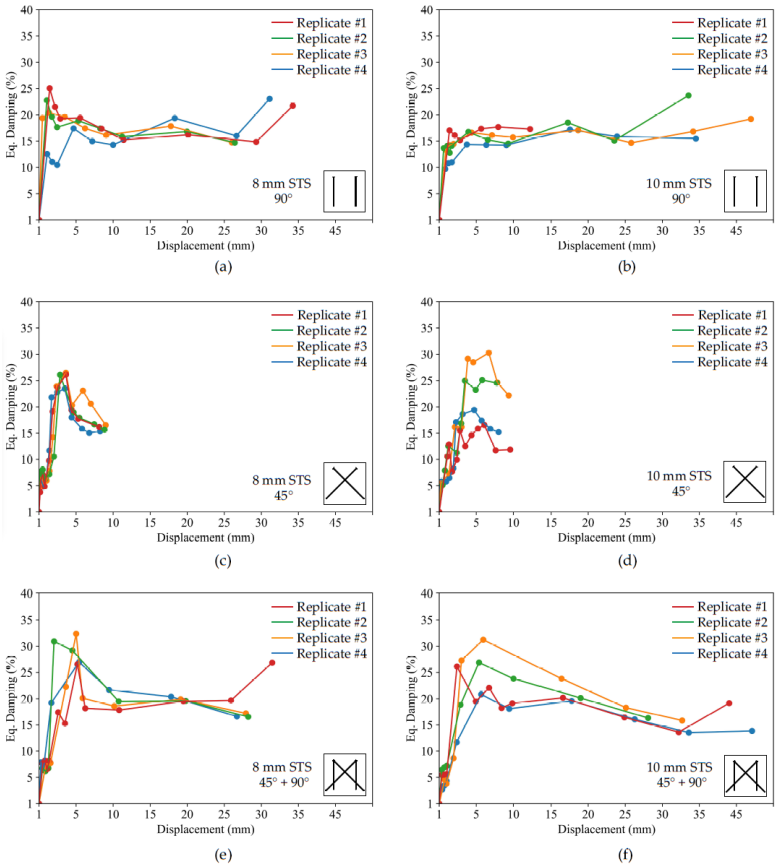

Figure 8. Equivalent viscous damping ratio of STS connections under reversed-cyclic loading: (**a**) 8 mm STS at 90°; (**b**) 10 mm STS at 90°; (**c**) 8 mm STS at 45°; (**d**) 10 mm STS at 45°; (**e**) 8 mm STS at mixed angles (45° and 90°); and (**f**) 10 mm STS at angles (45° and 90°).

4. Conclusions

Forty-eight self-tapping screw (STS) connections used to connect a CLT core to light-frame wood floor headers were tested under monotonic and reversed-cyclic load to investigate the strength, stiffness, ductility, and energy dissipation capacity of the connections. Three types of STS insertion angles were tested and compared: 45°, 90°, and mixed angles (90° and 45°). The results showed that all configurations of the connections have acceptable lateral load capacity and ductility. Furthermore, the connections with mixed angle STSs possessed high stiffness, ductility, and energy dissipation capacity and can be an efficient way to connect the light-frame wood structure to CLT cores under wind and seismic load. The detailed findings are summarized below:

- STSs were capable of transferring high lateral forces, which makes them feasible to be used in hybrid light-frame wood structures connected to CLT cores where a limited length of CLT core is available for installing the connections.
- Connections with 10 mm STSs had slightly higher strength than that with 8 mm STSs. However, 10 mm STSs were more prone to splitting wood; therefore, distance should be maintained between screws when they are connected to dimension lumber. Predrilling may also help prevent lumber splitting if enough distance cannot be guaranteed.
- 45° STS connections had greater stiffness but significantly lower ultimate displacement than 90° STS connections. It is recommended that these connections be detailed in accordance with capacity design principles and be regarded as non-dissipative (force-controlled) connections.
- Although the 90° STS connections had similar ductility to 45° STS connections, which is due to the definition of ductility ratio, their energy dissipation capacity was much larger than that of 45° STS connections.
- When combining 45° and 90° STSs in a connection, the system benefitted from the advantages of individual connection and made the STS joint a much more ductile connection.
- All test specimens provided acceptable energy dissipation capacity, as indicated by equivalent viscous damping values, which is not consistent with the conductions derived based on ductility ratio and energy dissipation values. Further research is needed to address this issue.

Author Contributions: Conceptualization, L.Z. and A.E.; methodology, L.Z. and C.N.; validation, L.Z. and C.N.; formal analysis, A.E.; investigation, A.E.; data curation, A.E.; writing—original draft preparation, A.E.; writing—review and editing, L.Z. and C.N.; visualization, A.E.; supervision, L.Z.; funding acquisition, L.Z. All authors have read and agreed to the published version of the manuscript.

Funding: This study was funded by Forestry Innovation Investment Ltd. through the BC Wood First Program, 21/22-UVIC-W22-043.

Institutional Review Board Statement: Not applicable.

Informed Consent Statement: Not applicable.

Data Availability Statement: Please email the corresponding author(s) to acquire data.

Acknowledgments: We express special thanks to Solomon Rosenberg, technician of the structures lab at the University of Victoria, for his valuable support; and many thanks are given to MTC solutions for their donations of STSs.

Conflicts of Interest: The authors declare no conflict of interest. The funders had no role in the design of the study; in the collection, analyses, or interpretation of data; in the writing of the manuscript, or in the decision to publish the results.

References

1. NBCC 2015. *National Building Code of Canada: Ottawa, Canadian Commission on Building and Fire Code*; National Research Council of Canada: Ottawa, ON, Canada, 2015.
2. Polastri, A.; Pozza, L.; Loss, C.; Smith, I. Numerical analyses of high- and medium-rise CLT buildings braced with cores and additional shear walls. *Struct. Archit.* **2016**, *5*, 128–136. [CrossRef]

3. Van de Lindt, J.W.; Asce, M. Evolution of Wood Shear Wall Testing, Modeling, and Reliability Analysis: Bibliography. *Pract. Period. Struct. Des. Constr.* **2004**, *1*, 44–53. [CrossRef]
4. Ceccotti, A.; Lauriola, M.P.; Pinna, M.; Sandhaas, C. SOFIE project-cyclic tests on cross-laminated wooden panels. In Proceedings of the 9th World Conference on Timber Engineering (WCTE), Portland, OR, USA, 6–10 August 2006.
5. Nguyen, T.T.; Dao, T.N.; Aaleti, S.; van de Lindt, J.W.; Fridley, K.J. Seismic assessment of a three-story wood building with an integrated CLT-lightframe system using RTHS. *Eng. Struct.* **2018**, *167*, 695–704. [CrossRef]
6. Anandan, Y.K.; van de Lindt, J.W.; Amini, M.O.; Dao, T.N.; Aaleti, S. Experimental Dynamic Testing of Full-Scale Light-Frame-CLT Wood Shear Wall System. *J. Archit. Eng.* **2021**, *1*, 04020042. [CrossRef]
7. Karacabeyli, E.; Gagnon, S. *Pîrvu, Canadian CLT Handbook: Cross-Laminated Timber*; FPInnovations: Québec, QC, Canada, 2019.
8. Loss, C.; Hossain, A.; Tannert, T. Simple cross-laminated timber shear connections with spatially arranged screws. *Eng. Struct.* **2018**, *173*, 340–356. [CrossRef]
9. Muñoz, W.; Mohammad, M.; Gagnon, S. Lateral and withdrawal resistance of typical CLT connections. In Proceedings of the 11th World Conference on Timber Engineering (WCTE), Riva del Garda, Italy, 20–24 June 2010.
10. Hossain, A.; Popovski, M.; Tannert, T. Cross-laminated timber connections assembled with a combination of screws in withdrawal and screws in shear. *Eng. Struct.* **2018**, *168*, 1–11. [CrossRef]
11. Tomasi, R.; Piazza, M.; Angeli, A.; Mores, M. A new ductile approach design of joints assembled with screw connectors. In Proceedings of the 9th World Conference on Timber Engineering (WCTE), Portland, OR, USA, 6–10 August 2006.
12. Gavric, I.; Fragiacomo, M.; Ceccotti, A. Cyclic behavior of typical screwed connections for cross-laminated (CLT) structures. *Eur. J. Wood Wood Prod.* **2015**, *2*, 179–191. [CrossRef]
13. Brown, J.R.; Li, M.; Tannert, T.; Moroder, D. Experimental study on orthogonal joints in cross-laminated timber with self-tapping screws installed with mixed angles. *Eng. Struct.* **2021**, *228*, 111560. [CrossRef]
14. *CSA O86*; Engineering Design in Wood. Canadian Standard Association: Toronto, ON, Canada, 2019.
15. MTC. Solutions. Structural Screw Design Guide 2019. In *Pîrvu, Canadian CLT Handbook: Cross-Laminated Timber*; Karacabeyli, E., Gagnon, S., Eds.; FPInnovations: Vancouver, BC, Canada, 2020.
16. *ANSI/APA PRG 320*; Standard for Performance-rated Cross Laminates Timber. American National Standards Institute, The Engineered Wood Association: New York, NY, USA, 2018.
17. CCMC. *Evaluation Report SWG ASSY®VG Plus and SWG ASSY®3.0 Self-Tapping Wood Screws*; CCMC: Ottawa, ON, Canada, 2020.
18. *ASTM D1761*; Standard test Methods for Mechanical Fasteners in Wood. American Society for Testing Material Standard: West Conshohocken, PA, USA, 2020. [CrossRef]
19. *ASTM E2126*; Standard Test Methods for Cyclic (Reversed) Load Test for Shear Resistance of Vertical Elements of the Lateral Force Resisting Systems for Buildings. American Society for Testing Material Standard: West Conshohocken, PA, USA, 2019. [CrossRef]
20. Varum, H.S.A. Seismic Assessment, Strengthening and Repair of Existing Buildings. Doctoral Dissertation, Universidade de Aveiro, Aveiro, Portugal, 2003.